



# Biosorption of Rhodamine B dye from aqueous solution by *Rhus coriaria* L. plant: Equilibrium, kinetic, thermodynamic and DFT calculations

Muhammed Safa Çelik<sup>1</sup>, Şenay Akkuş Çetinus<sup>2</sup>, Ali Fazıl Yenidünya<sup>1</sup>, Serap Çetinkaya<sup>1</sup>, Burak Tüzün<sup>3,\*</sup>

<sup>1</sup> Department of Molecular Biology and Genetics, Science Faculty, Sivas Cumhuriyet University, Sivas, Turkey

<sup>2</sup> Department of Biochemistry, Faculty of Science, Sivas Cumhuriyet University, Sivas Turkey

<sup>3</sup> Plant and Animal Production Department, Technical Sciences Vocational School of Sivas, Sivas Cumhuriyet University, Sivas, Turkey



## ARTICLE INFO

### Article history:

Received 15 June 2022

Revised 7 September 2022

Accepted 13 September 2022

Available online 16 September 2022

### Keywords:

Biosorption

DFT

Rhodamine B

*Rhus coriaria* L. (Anacardiaceae)

## ABSTRACT

Water-soluble basic rhodamine B (RhB) was adsorbed onto fruit powders of *Rhus coriaria* L. (Anacardiaceae), sumac in batch reactions. Adsorption was optimized by employing concentration, pH, and time parameters. Experimental data were in accordance with the Freundlich isotherm, adsorption obeyed the pseudo-second-order kinetics, and thermodynamic parameters indicated that adsorption was exothermic, spontaneous, and chemical. Results were also evaluated by theoretical means: lowest Unoccupied Molecular Orbitals (LUMO), and the Highest Occupied Molecular Orbitals (HOMO). The HOMO energy values of the rhodamine B molecule had the highest activity with  $-3.3729$  at the B3LYP level,  $-6.0361$  at the HF level, and  $-4.3299$  at the M062X level. In the calculations made, it was seen that the rhodamine B molecule has more electron density on the oxygen molecules. Taken together, the findings suggested that the dried fruit of the *Rhus coriaria* L. could be a useful biosorbent for the removal of dyes from aqueous media.

© 2022 Elsevier B.V. All rights reserved.

## 1. Introduction

Dyes are widely used in many industrial applications, including cosmetics, dyeing, food processing, leather, paint manufacturing, paper and textile industries. These common facilities produce coloured wastewater. Since many of the industrial dyes are non-biodegradable due to their chemical structure and molecular size, they have become a major environmental concern around the world [1]. Most of these dyes cause serious health problems [2,3], as they disrupt the natural cycling of the food chain in rivers and oceans [4].

There exist various methods for trapping waste dye from industrial outlets. Biological processes, for example, aerobic oxidation and/or anaerobic digestion, are not efficient against colour compounds harbouring aromatic rings, amine groups, sulfonic groups, or metal ions [5–7]. On the other hand, conventional physicochemical processes such as adsorption, coagulation/flocculation, advanced oxidation processes, ozonation, electrokinetic coagulation, electrochemical degradation, electroflotation, ion exchange, irradi-

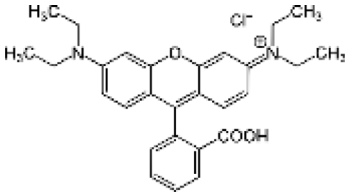
ation, membrane filtration, and precipitation are highly efficient suitable for small-scale industries [5,8]. Their high cost, notwithstanding, makes them less preferable. Thus, biosorption processes often relying on naturally occurring low-cost polymers now seem to have taken the edge off this surmounting problem of pollution [9].

Biosorption, a relatively novel approach, can be defined as the separation of organic and inorganic species, including metals, dyes, and odour-causing substances, using live cells or parts of their biomass, such as bacteria, fungi, seaweed, various sludge materials, or byproducts of the fermentation industries. Recent studies have identified many biosorbent organisms such as green alga *Enteromorpha* [10], *Platanus orientalis* [11], rice husk [12] *Paspalum notatum* [13], and *Posidonia oceanica* [14–16].

In addition, comparing the activities of my molecules by calculating chemical parameters using theoretical calculations has become much easier now. Developing technology and breakthroughs have improved both programs and computers. Gaussian package program was used for these calculations [17,18]. Comparison of the activities of the studied molecule 2a-2i was made. B3LYP, HF, M06-2x methods with the 6-31++g(d,p) basis sets were used for the calculations. The use of theoretical methods based on density func-

\* Corresponding authors: [theburaktuzun@yahoo.com](mailto:theburaktuzun@yahoo.com)  
E-mail address: [btuzun@cumhuriyet.edu.tr](mailto:btuzun@cumhuriyet.edu.tr) (B. Tüzün).

**Table 1**  
Chemical characteristics of RhB.

Dye	Molecular Structure	Chemical Formula
Rhodamine B		C <sub>28</sub> H <sub>31</sub> ClN <sub>2</sub> O <sub>3</sub>

tional theory (DFT) is a robust tool that provides important information about the chemical, electronic, and physical properties of molecules and allows to explain their biological activities [19].

Sumac has only been used twice before and the adsorbate is methylene blue. The effects of dye concentration, initial solution pH and phase contact time were investigated in both studies [20, 21].

In the present study, the dried and ground fruit of *Rhus coriaria* L. plant, sumac, was used for the adsorption of water-soluble basic Rhodamine B (RhB). The ripe fruit is spherical, hairy, red coloured, and has a sour flavour. It is an antibacterial fruit but it has mostly been a renowned spice and molasses ingredient. It has also long been a convenient source of a natural dye for the traditionally produced cotton- and wool fibres. Biosorption on this fruit material was carried out in batch reactions by optimising a number of operating variables: adsorption time and temperature, concentration of the adsorbate, and pH. The mechanism of RhB retention was attempted to be clarified by both experimental and theoretical means.

**Fig. 1.** *Rhus coriaria* L. plant.

## 2. Materials and methods

### 2.1. Chemicals

Rhodamine B (RhB), ethanol (EtOH), hydrochloric acid (HCl), sodium hydroxide (NaOH) used in the experiments were of analytical grade and were obtained from Merck and Sigma-Aldrich companies.

Rhodamine B (Basic Violet 10, Table 1), a phototoxic and photoallergic dye substance, is a water-soluble organic dye widely used for industrial purposes. It is known to be harmful if swallowed and may cause eye-, skin-, and respiratory tract irritation [22].

### 2.2. Biosorbent preparation

The fruit (Şehitkamil, Gaziantep, Turkey) was collected from the leatherman sumac plant (*Rhus coriaria* L.) in September 2021 (Fig. 1). It was washed in distilled water in the laboratory, dried for 48h at 70°C. Dry biomass was ground with a blender and used as the adsorbent.

### 2.3. Preparation of RhB solution

A RhB stock solution was prepared at 1,0 g/L in water. Dilutions of this solution were used in the experiments. Concentrations were read at 558 nm (UV-Vis spectrophotometer, T60, China).

### 2.4. Biosorbent characterization

Surface functional groups of the biosorbent were inspected by Fourier Transform Infrared (FT-IR) Spectrometer (ATR, Bruker, Tensor II) before and after biosorption reactions. Surface morphology, again biosorbent before and after biosorption, were visualized by scanning electron microscopy (SEM) and energy dispersive x-ray

(EDX) spectroscopy (TESCAN MIRA3 XMU) at CÜTAM Central Laboratory of Sivas Cumhuriyet University, Turkey).

### 2.5. Batch biosorption experiments

Biosorption of RhB on *Rhus coriaria* L. fruit was investigated in 10 ml batch biosorption reaction volume using the recipe as follows: fruit powder, 50 mg; RhB, 100 mg L<sup>-1</sup> at natural pH (pH 6.36) of RhB dye at 25°C and with an incubation time for 24h. The initial pH of the biosorption solution was studied in the range of 5.0-8.0. Parameters such as 0.01-0.5 g biosorbent dosage range, initial concentration of 1-10 mg/L RhB solution, contact time between 0-1440 min were studied at 25°C. RhB concentration was checked periodically at 558 nm [23].

### 2.6. DFT method

Abstract designs offer helpful data on the elemental and organic features of particles and numerous elemental quantum constraints can be visualized through them. In the production of such data a few software programs have been made available: Gaussian09 RevD.01 [24], and GaussView 6.0 [25] in which B3LYP, HF, M06-2x [26-28] methods with the 6-31++g(d,p) could be used, and calculations on HOMO (Highest Occupied Molecular Orbital), LUMO (Lowest Unoccupied Molecular Orbital), ΔE (HOMO-LUMO energy gap), chemical potential (μ), electrophilicity (ω), chemical hardness (η), global softness (σ), Many parameters such as nucleophilicity (ε), dipole moment, and energy value were possible [29,30].

$$\chi = -\left(\frac{\partial E}{\partial N}\right)_{v(r)} = \frac{1}{2}(I + A) \cong -\frac{1}{2}(E_{HOMO} + E_{LUMO}) \quad (1)$$

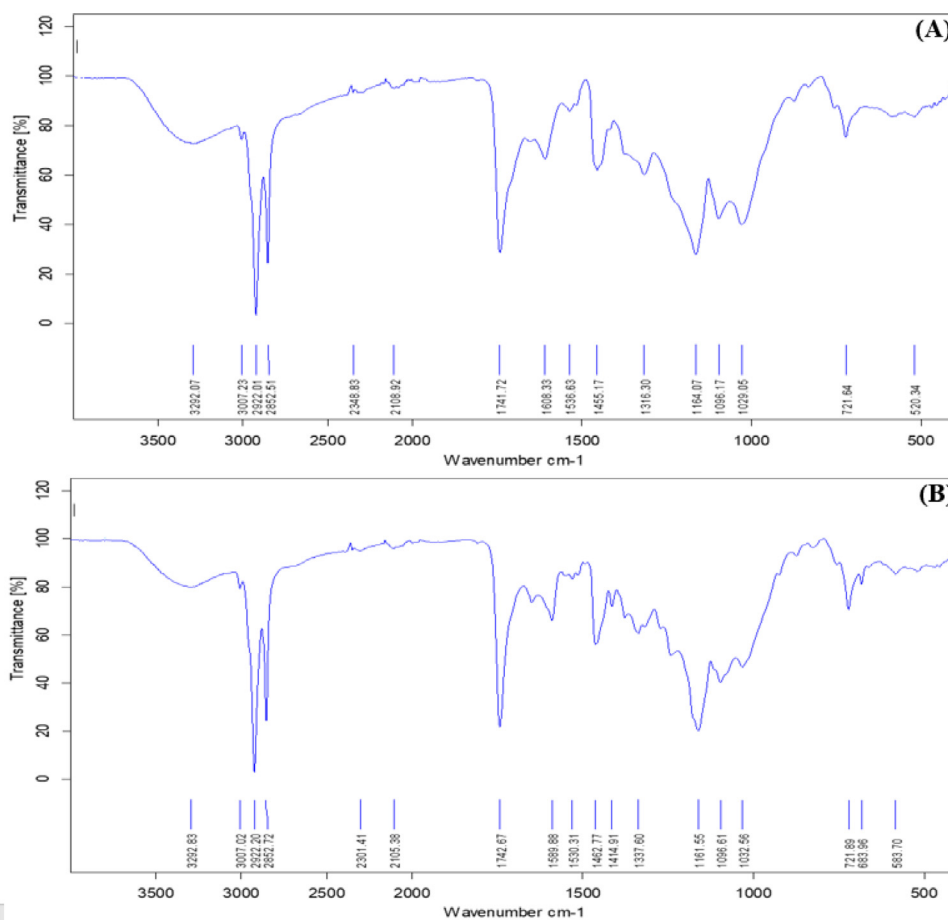


Fig. 2. FT-IR spectrum of unloaded and RdB loaded *Rhus coriaria* L.

$$\eta = -\left(\frac{\partial^2 E}{\partial N^2}\right)_{v(r)} = \frac{1}{2}(I - A) \cong -\frac{1}{2}(E_{HOMO} - E_{LUMO}) \quad (2)$$

$$\sigma = 1/\eta \quad \omega = \chi^2/2\eta \quad \varepsilon = 1/\omega \quad (3)$$

### 3. Results and discussion

#### 3.1. FT-IR and SEM-EDX analyses

Empty functional groups were detected by FT-IR before and after biosorption (Figs. 2a and 2b, respectively). The fruit of *Rhus coriaria* L. had several -OH groups on the ring that were represented by the broad band at 3292 cm<sup>-1</sup>. The weak peaks at 2922 and 2852 cm<sup>-1</sup> were aliphatic ν(C-H) stretching vibrations. Asymmetric stretching vibrations of the ν(COO) groups were registered at 1741 cm<sup>-1</sup> and 1608 cm<sup>-1</sup>. Aromatic C = C stretching vibrations appeared between 1536 and 1455 cm<sup>-1</sup>.

It was evident that after biosorption some slight shifts occurred in the initial FT-IR peaks and a new (C-S-C) stretching appeared on RhB at 683 cm<sup>-1</sup> (Fig. 2b).

While the surface morphology of the biosorbent was quite rough before adsorption, the roughness decreased afterward (Figs. 3a and 3b, respectively). This evidence also indicated that adsorption process was successful. EDX spectra indicated the existence of C, N, and O elements before adsorption. After adsorption, besides the appearance of Cl, the percentages of CN and O appeared to have increased (Figs. 3c and 3d, respectively). Taken together, the analytical and visual data produced concordant results [31].

#### 3.2. Biosorption procedure and modelling of biosorption process

The amount of dye adsorbed per gram of adsorbent (Q) was calculated from the equation below by using the calibration curve containing the absorbance values against the increasing dye concentration:

$$Q = \frac{(C_0 - C_s)}{m} \times V \quad (4)$$

Q: Adsorbed dye (mg dye/g adsorbent)

C<sub>0</sub>: Initial concentration of the dye (mg/L)

C<sub>s</sub>: Equilibrium concentration of the dye (mg/L) (dye concentration of the solution after adsorption)

V: Solution volume (L)

m: Adsorbent (fruit) mass.

As the equilibrium concentration (C<sub>s</sub>) of the dye increased, the amount of dye adsorbed (Q) by per gram of adsorbent also increased. It was observed that a maximum of 0.90-0.98 mg of dye was adsorbed by per gram of adsorbent (Fig. 4).

Adsorption conforms to the Freundlich isotherm.

$$Qe = K_f \times C_s^{1/n} \quad (5)$$

$$\ln Qe = \ln K_f + \frac{1}{n} \ln C_s \quad (6)$$

Freundlich isotherm analysis was carried out using Equation 3. Here, lnC<sub>s</sub> versus lnQe was plotted linearly (Fig. 5), and the slope of this graph and the cut-off point K<sub>f</sub> and n values were calculated (Table 2).

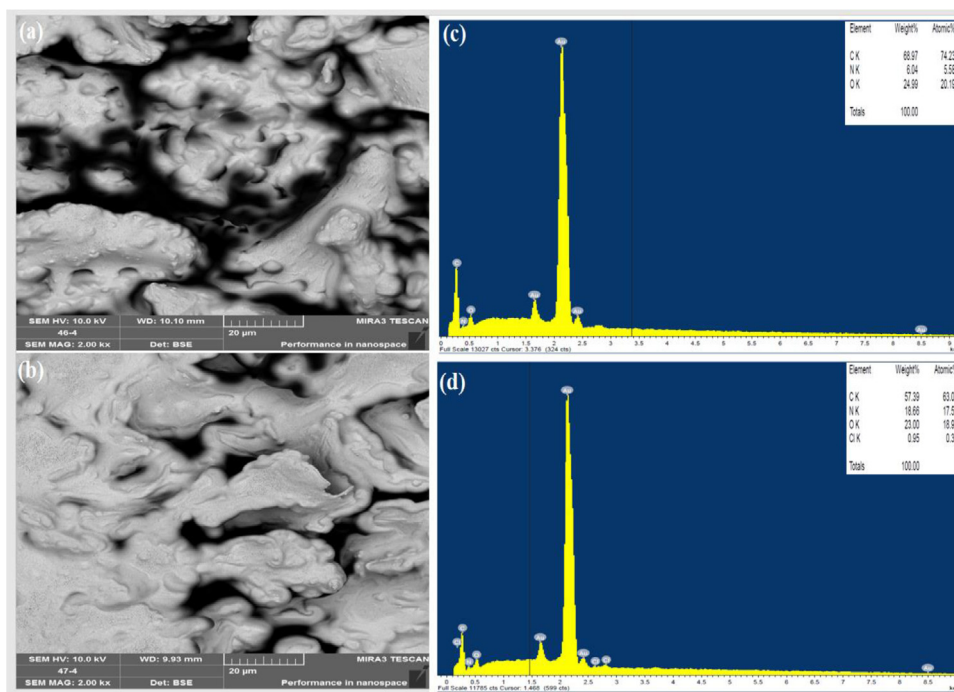


Fig. 3. SEM images of RhB biosorption before (a) and after (b) and EDX spectrums of RhB biosorption before (c) and after (d).

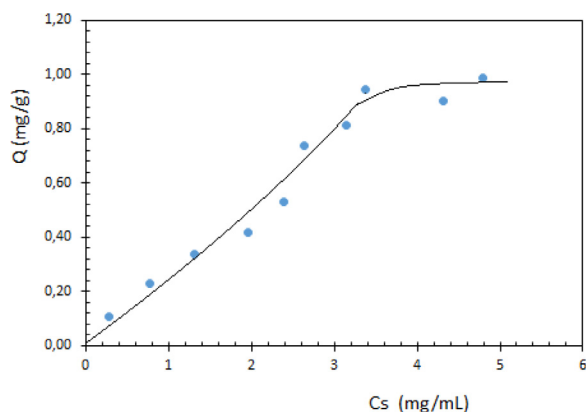


Fig. 4. Experimental biosorption isotherm.

Table 2  
Experimental values of the Freundlich isotherm.

$K_f ((\text{mg g}^{-1})(\text{L mg}^{-1})^{1/n})$	$1/n$	$n (\text{g L}^{-1})$	$R^2$	Isotherm type
0,288	0,8234	1,21	0,9739	L

Here,  $K_f ((\text{mg g}^{-1})(\text{L mg}^{-1})^{1/n})$  and  $n$  were Freundlich equation constants, related to adsorption capacity and density, respectively. Freundlich's constant was equal to the adsorption capacity at  $C=1$ . High  $K_f$  value indicated that the adsorbent adsorbed the solution easily. The type of the process was determined by the parameter  $n$ . If  $n=1$ , the process is linear, chemical when  $n>1$ , and physical when  $n<1$ . In addition,  $n$  is a measure of the deviation of the isotherm from the linearity and is a factor of heterogeneity. The  $n$  value defines S, L and C type isotherms in Giles adsorption isotherm classification. If  $n<1$  indicates S type,  $n=1$  indicates C type, if  $n>1$  indicates L type isotherm [32, 33]. As with all plants, cellulose provides structural strength to sumac. This polymer is formed  $\beta$ -1,4 glucosidic bonds between glucose monomers. At neutral pH, the OH groups in cellulose could interact with the

carbonyl oxygen ( $-\text{C}=\text{O}$ ) of RB and thus participate in the adsorption process through hydrogen bonds.

### 3.3. Effect of temperature and biosorption thermodynamic studies

Thermodynamic studies were carried out at four different temperatures, 25°C, 30°C, 35°C and 40°C. Changes in Standard free energy ( $\Delta G^\circ$ ), enthalpy ( $\Delta H^\circ$ ) and entropy ( $\Delta S^\circ$ ) were found using the equations below:

$$K_d = \frac{(C_0 - C_s)}{C_s} = \frac{Q_d}{C_s} \quad (7)$$

( $C_0 - C_s$ ), quantity of dye adsorbed at equilibrium ( $\text{mg L}^{-1}$ );  $C_s$  dye particles left after the adsorption ( $\text{mg L}^{-1}$ ); and  $K_D$ , adsorption equilibrium constant at a given temperature. Gibbs free energy was established using Equation 8 (Table 3) [34]:

$$\Delta G^\circ = -RT \ln K_D \quad (8)$$

$\Delta H^\circ$  and  $\Delta S^\circ$  were worked out by Equation 9 (Van't Hoff equation):

$$\ln K_D = \frac{\Delta S^\circ}{R} - \frac{\Delta H^\circ}{RT} \quad (9)$$

$R$  ( $8.314 \text{ J mol}^{-1} \text{ K}^{-1}$ ), gas constant, and  $T$  (K), absolute temperature.

Here,  $1/T$  versus  $\ln K_D$  was plotted linearly (Fig. 6), and  $\Delta H^\circ$  and  $\Delta S^\circ$  were computed as indicated (Table 3) [35,36].

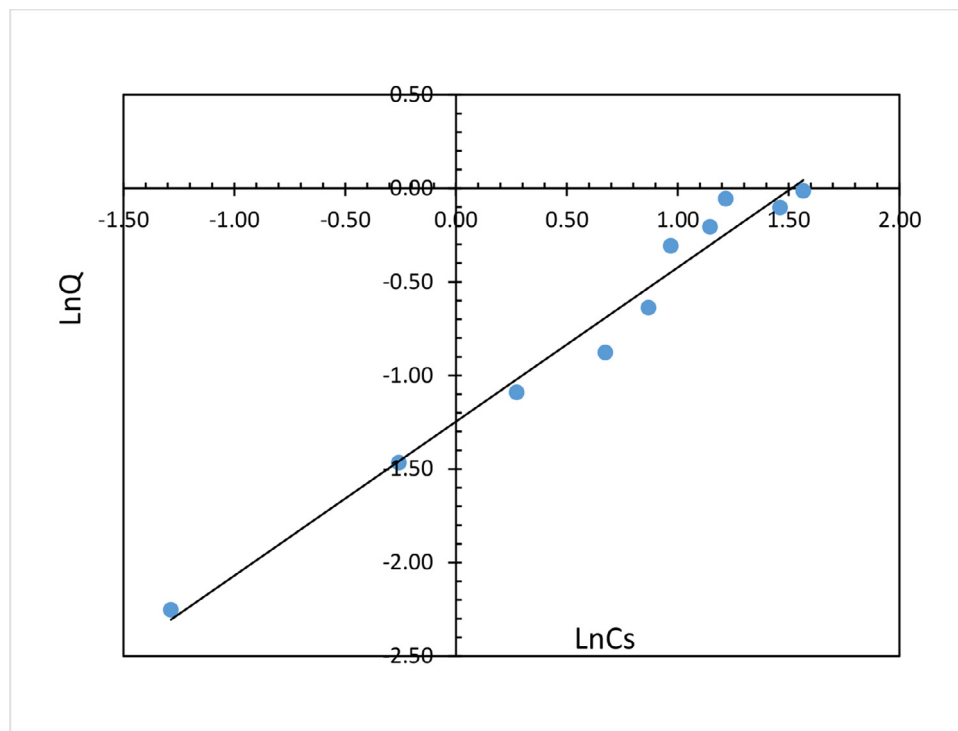
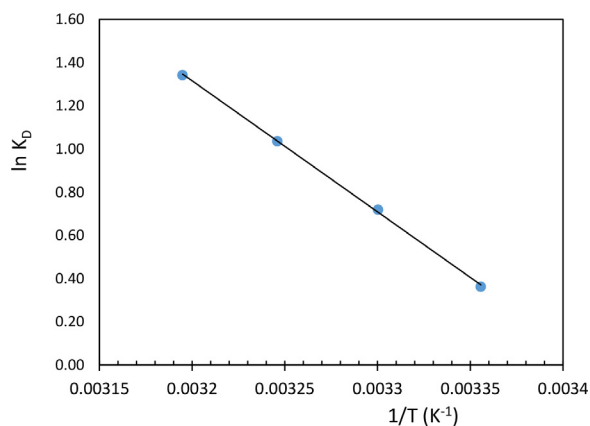
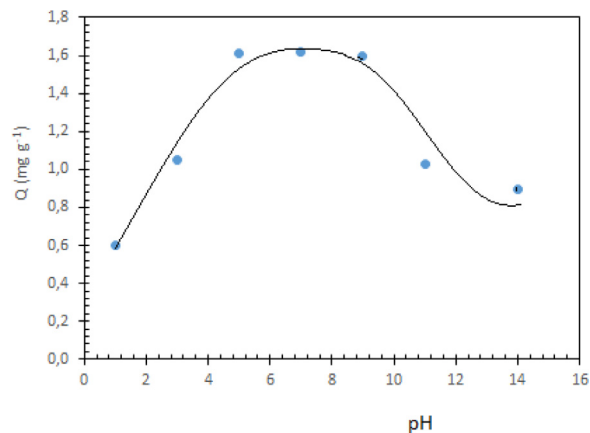
Experimental data (Table 3) suggested that a spontaneous, endothermic adsorption took place.

### 3.4. Effect of pH

Adsorption appeared to be dependent on pH (Fig. 7), as it was observed that adsorption increased at elevated pH points, up to 10. Maximum absorbance spanned a slightly acidic and slightly basic ends, between pH 5 and 9. It has been previously stated that hydrogen bonds may form between the carbonyl oxygen in RB and the hydroxyl group hydrogen of sumac cellulose. The ionization of

**Tablo 3**  
Thermodynamic parameters of bioadsorption.

Temperature (°C)	$K_D$	Slope	Cut off point	$R^2$	$\Delta G^\circ(\text{J mol}^{-1})$	$\Delta H^\circ(\text{kJ mol}^{-1} \text{K}^{-1})$	$\Delta S^\circ(\text{J mol}^{-1} \text{K}^{-1})$
25	1,437				-898		
30	2,054	-6069,2	20,4738	0,9995	-1813	50,56	173
35	2,820				-2654		
40	3,830				-3495		

**Fig. 5.** Freundlich isotherm model**Fig. 6.** Van't Hoff equation graph.**Fig. 7.** pH range of the adsorption.

the carboxyl group takes place below pH 5. At higher pH points, carboxyl group of RB becomes ionized by releasing its hydrogen. Between pH 5 and pH 9, this negatively charged group might then contribute to the adsorption through electrostatic attractions with the positively charged sumak proteins. Below pH 5 and above 9, on the other hand, the adsorption rate is expected to decrease through repulsive interactions between the respective groups.

### 3.5. Biosorbent mass effect

In the adsorption only the adsorbent mass was varied. Thus, it was as expected observed that the amount of dye adsorbed by per gram of adsorbent decreased against increasing adsorbent masses at fixed dye concentrations (Fig. 8). This decrease could be due to the incomplete filling on the biosorbent surface. This could be demonstrated by increasing the concentration of the adsorbate



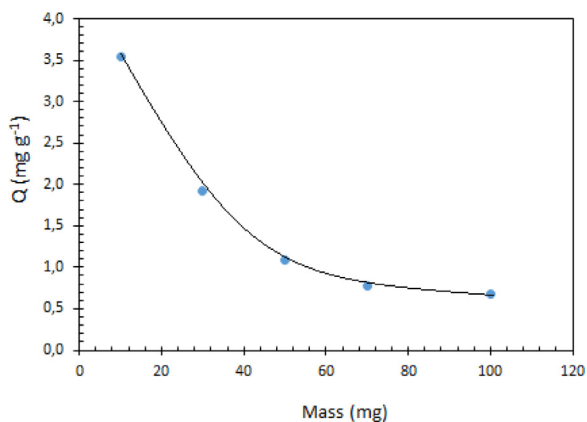


Fig. 8. Effect of adsorbent mass on adsorption.

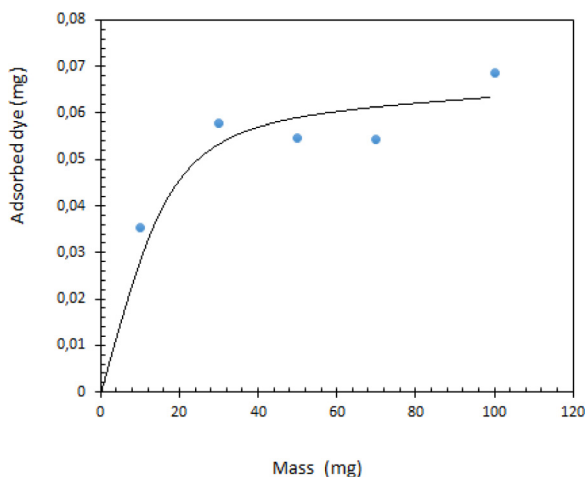


Fig. 9. The amount of dye adsorbed against the adsorbent mass.

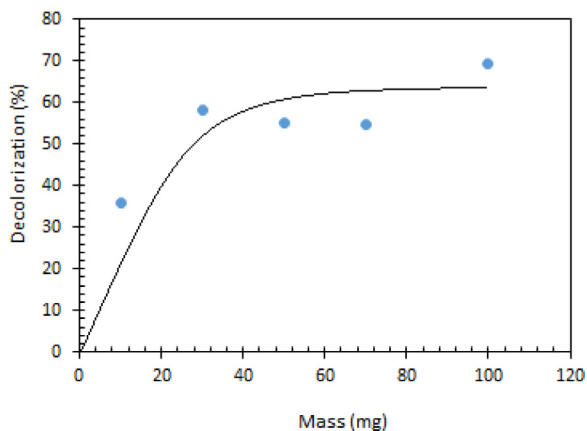


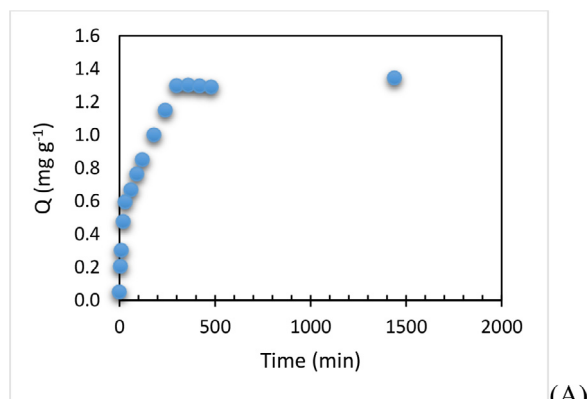
Fig. 10. Percentage of colour removal versus adsorbent mass.

[37] as SEM micrographs informed the incomplete filling of the biosorbent surface.

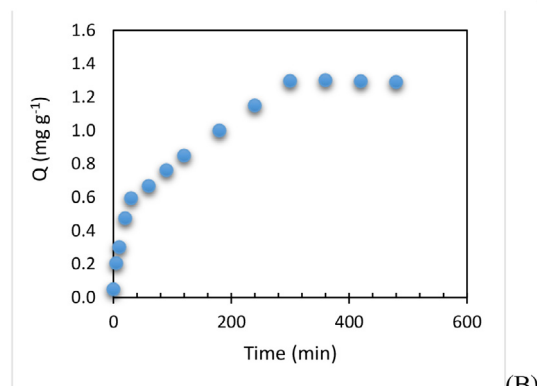
The amount of dye adsorbed (Fig. 9) and percentage of dye removal (Fig. 10) were also calculated against the increase in adsorbent mass, and it was found that the adsorbent between 40 and 100 mg showed maximum adsorption at fixed dye concentration.

### 3.6. Effect of contact time and kinetic on biosorption

Adsorption was observed for 1440 min (24 hours) by keeping adsorbent mass, dye concentration and solution volume constant



(A)



(B)

Fig. 11. Adsorption curve against time.

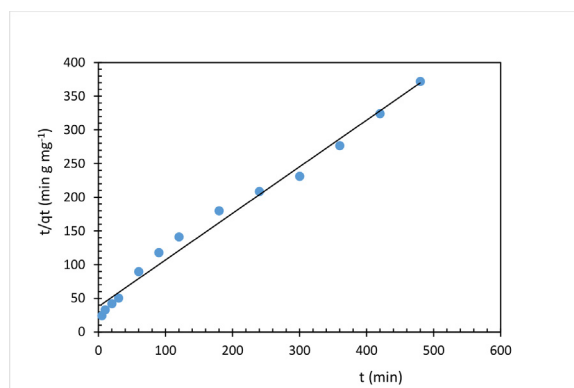


Fig. 12. The graph of pseudo-second-order kinetic model.

Table 4  
Pseudo-second-order kinetic parameters.

$k_2$ (mg g <sup>-1</sup> min <sup>-1</sup> )	$Q_e$ (mg g <sup>-1</sup> ) (theoretical)	$Q_e$ (mg g <sup>-1</sup> ) (experimental)	R <sup>2</sup>
0,0127	1,446	1,309	0,987

(Fig. 11) and it was noted that adsorption reached its maximum (1.30 mg g<sup>-1</sup>) in 300 min (5 hours).

In this study, two different kinetic models were used, namely the pseudo-first-order equation (Pseudo-First-Order Equation) and the pseudo-second-order equation (Pseudo-Second-Order Rate Equation) [38].

Pseudo-First-Order Equation:

$$\log(Q_e - Qt) = \log Q_e - \frac{k_1}{2,303} t \tag{10}$$

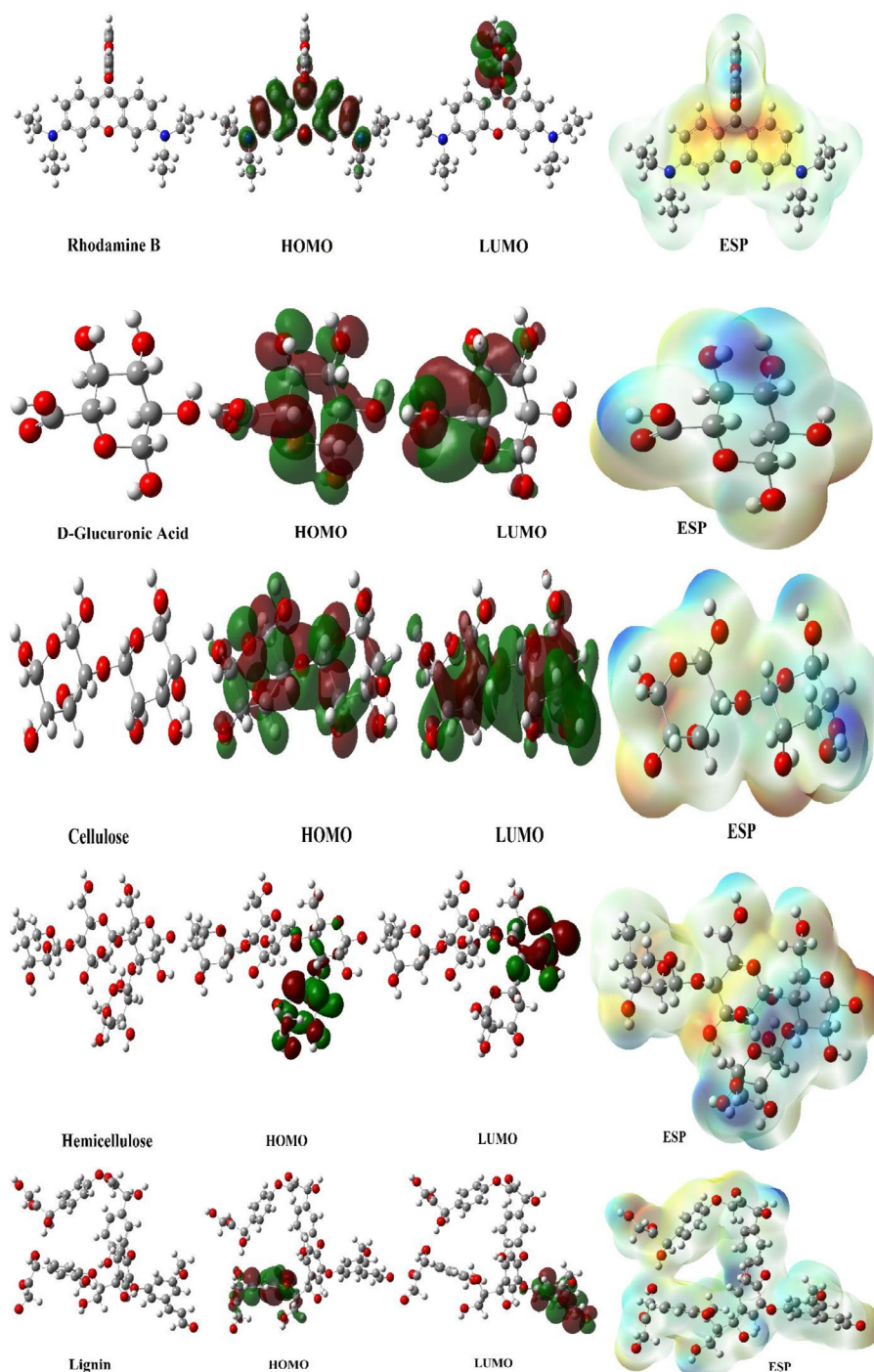


**Fig. 13.** A representation of optimized structures, HOMO, LUMO, and ESP shapes of molecules.

Here,  $Q_e$  ( $\text{mg g}^{-1}$ ) and  $Q_t$  ( $\text{mg g}^{-1}$ ) were the adsorption capacities at equilibrium and any  $t$  time, respectively, and  $k_1$  ( $\text{min}^{-1}$ ), the pseudo first-order rate constant [39].

Against  $t$ ,  $\log(Q_e - Q_t)$  values were plotted linearly and the slope of this line and the cut-off point of  $k_1$  and  $Q_e$  values were calculated. The low  $R^2$  value (0.839) indicated that the adsorption did not comply with the pseudo-first order kinetics.

*Pseudo-Second-Order Rate Equation:*

$$\frac{t}{Q_t} = \frac{1}{k_2 Q_e^2} + \frac{1}{Q_e} x t \quad (11)$$

$k_2$  ( $\text{g mg}^{-1} \text{min}^{-1}$ ): pseudo second order rate constant

Here,  $t/q_t$  values against  $t$  are plotted (Fig. 12) and  $k_2$  and  $Q_e$  values were calculated from the slope and segment of this line (Table 4) [39]. The graph showed that the kinetics of the adsorption fitted to pseudo-second order because the  $R^2$  value was higher (0.987).

### 3.7. Theoretical results

There are many parameters calculated as a result of Gaussian calculations. The numerical values of these parameters can be used to describe the activities of molecules. Each calculated parameter provides information about a different property of the molecules.

**Table 5**

The calculated quantum chemical parameters of molecules.

	$E_{\text{HOMO}}$	$E_{\text{LUMO}}$	I	A	$\Delta E$	$\eta$	$\mu$	$\chi$	Pi	$\omega$	$\varepsilon$	dipol	Energy
<b>B3LYP/6-31++G(d,p) LEVEL</b>													
1	-3.3729	-1.4234	3.3729	1.4234	1.9494	0.9747	1.0259	2.3982	-2.3982	2.9502	0.3390	1.6928	-38652.7513
2	-7.7575	-1.0278	7.7575	1.0278	6.7297	3.3649	0.2972	4.3926	-4.3926	2.8672	0.3488	3.5589	-20711.3247
3	-7.2568	-0.7440	7.2568	0.7440	6.5128	3.2564	0.3071	4.0004	-4.0004	2.4572	0.4070	5.0380	-33174.4174
4	-6.8783	-0.8757	6.8783	0.8757	6.0026	3.0013	0.3332	3.8770	-3.8770	2.5041	0.3994	6.0626	-64433.2566
5	-6.1664	-2.3777	6.1664	2.3777	3.7887	1.8943	0.5279	4.2721	-4.2721	4.8172	0.2076	5.0369	-86315.6278
<b>HF/6-31++G(d,p) LEVEL</b>													
1	-6.0361	1.0626	6.0361	-1.0626	7.0987	3.5493	0.2817	2.4867	-2.4867	0.8711	1.1479	1.3385	-38407.6524
2	-11.7810	0.8928	11.781	-0.8928	12.6738	6.3369	0.1578	5.4441	-5.4441	2.3385	0.4276	3.8813	-20597.9992
3	-10.9546	0.9040	10.954	-0.9040	11.8585	5.9293	0.1687	5.0253	-5.0253	2.1296	0.4696	5.4632	-32991.2669
4	-10.6672	0.7720	10.667	-0.7720	11.4392	5.7196	0.1748	4.9476	-4.9476	2.1399	0.4673	5.9051	-64068.0607
5	-8.5300	0.7070	8.5300	-0.7070	9.2370	4.6185	0.2165	3.9115	-3.9115	1.6564	0.6037	8.6909	-85807.2190
<b>M062X/6-31++G(d,p) LEVEL</b>													
1	-4.3299	-0.3867	4.3299	0.3867	3.9432	1.9716	0.5072	2.3583	-2.3583	1.4104	0.7090	1.5641	-38635.7335
2	-9.5126	-2.7651	9.5126	2.7651	6.7475	3.3738	0.2964	6.1389	-6.1389	5.5851	0.1790	4.5215	-20703.3824
3	-8.9425	-0.4234	8.9425	0.4234	8.5191	4.2596	0.2348	4.6830	-4.6830	2.5742	0.3885	5.0405	-33161.9510
4	-8.5537	-0.5418	8.5537	0.5418	8.0119	4.0060	0.2496	4.5477	-4.5477	2.5814	0.3874	6.1603	-64408.3553
5	-6.3066	-0.0487	6.3066	0.0487	6.2579	3.1289	0.3196	3.1776	-3.1776	1.6135	0.6198	8.2760	-86489.8903

Two of the most important of these parameters are the Lowest Unoccupied Molecular Orbitals (LUMO), which is used to explain the electron accepting feature of this molecule, and the Highest Occupied Molecular Orbitals (HOMO), which is used to explain the electron donating feature of this molecule, which two parameters can be used to compare activity [40–43]. The activities of rhodamine B (1), D-glucuronic acid (2), cellulose (3), hemicellulose (4), and lignin (5) molecules, which are obtained as a result of the calculations, are compared. It has been determined that the rhodamine B (1) molecule has higher activity due to its HOMO energy numerical value being more positive than other molecules at all levels.

Apart from these two calculated parameters, many parameters are calculated. The first of these is the energy gap parameter, which is an important parameter that shows the energy difference between the numerical values of the HOMO and LUMO parameters [42–45]. When the electronegativity values of the molecules were matched, it was seen that rhodamine B (1) has higher activity due to its lower electronegativity numerical value than other molecules at all levels.

When the equations given in the method section of the other parameters are taken into consideration, it is seen that a similar order is obtained since all other parameters are obtained from the numerical values of the HOMO and LUMO parameters. In experimental biological activity studies, when comparing the activity of molecules, it should be well known that the chemical interactions of molecules in biological materials determine the activity [46–48].

As could be seen in the numerical values of the HOMO parameters (Table 5), rhodamine B molecule 1 appeared to have the highest HOMO energy values, and its LUMO values seemed to be more widely ranged. The lowest  $\Delta E$  parameter value also indicated its higher kinetic activity. It was inferred from these parameters that rhodamine B molecule no. 1 had the highest bonding activity [49, 50].

Some parameters were represented in four different images (Fig. 13). The first of these was the optimized shapes of molecules. Two of the images were used to indicate HOMO or LUMO orbitals. Electron donating and accepting regions were shown in red and blue, respectively [51,52].

#### 4. Conclusion

From this study, it was found that the dried fruit of *Rhus coriaria* L. could be a useful biosorbent for the removal of dyes from aqueous media, and the following conclusions were made from this study:

- Experimental data were in accordance with the Freundlich isotherm,
- Adsorption obeyed the pseudo-second-order kinetics
- Thermodynamic parameters indicated that adsorption was exothermic, spontaneous, and chemical.

The theoretical calculations made are an important method to compare the activities of molecules. When the results of these calculations are examined, it is seen that the HOMO energy values of the rhodamine B molecule have the highest activity with -3.3729 at the B3LYP level, -6.0361 at the HF level, and -4.3299 at the M062X level. In the calculations made, it was seen that the rhodamine B molecule has more electron density on the oxygen molecules. It will be thought that it will interact through these oxygen atoms.

As mentioned above, in the literature, only two studies have used sumac material for dye removal. The obtained results show that the material used is a suitable adsorbent for adsorption.

#### Credit Author Statement

**Muhammed Safa Çelik:** Methodology, Validation,  
**Şenay Akkuş Çetinus:** Methodology, Validation, Writing - Original Draft, Writing - Review & Editing  
**Ali Fazıl Yenidünya:** Methodology, Validation, Writing - Original Draft, Writing - Review & Editing  
**Serap Çetinkaya:** Methodology, Validation, Methodology, Validation, Writing - Review & Editing,  
**Burak Tüzün:** Methodology, Software, Validation, Writing - Original Draft, Writing - Review & Editing

#### Declaration of Competing Interest

The authors declare that they have no known competing financial interests or personal relationships that could have appeared to influence the work reported in this paper.

#### Data Availability

No data was used for the research described in the article.

#### Acknowledgments

The numerical calculations reported in this paper were fully/partially performed at TUBITAK ULAKBIM, High Performance and Grid Computing Center (TRUBA resources).



## References

- [1] H. Keharia, D. Madamwar, Bioremediation concepts for treatment of dye containing wastewater: A review, *Indian J. Exp. Biol.* 41 (2003) 1068–1075.
- [2] Z. Bekci, Y. Sekia, L. Cavas, Removal of malachite green by using an invasive marine algae *Caulerpa racemosa* var. *clyndracea*, *J. Hazard. Mater.* 161 (2009) 1454–1460, doi:10.1016/j.jhazmat.2008.04.125.
- [3] J.H. Sun, S.P. Sun, G.L. Wang, L.P. Qiao, Degradation of azo dye Amido black 10B in aqueous solution by Fenton oxidation process, *Dyes Pigm.* 74 (2007) 647–652, doi:10.1016/j.dyepig.2006.04.006.
- [4] E. Daneshvar, M. Kousha, N. Koutahzadeh, M.S. Sohrabi, A. Bhatnagar, Biosorption and bioaccumulation studies of acid orange 7 dye by *Ceratophyllum demersum*, *Environ. Prog. Sustain. Energy* 32 (2) (2013) 285–293, doi:10.1002/ep.11623.
- [5] M. Asgher, Biosorption of reactive dyes: A review, *Wat. Air and Soil Poll.* 223 (5) (2012) 2417–2435, doi:10.1007/s11270-011-1034-z.
- [6] C.R. Corso, E.J.R. Almeida, G.C. Santos, L.G. Morão, G.S.L. Fabris, E.K. Mitter, Bioremediation of direct dyes in simulated textile effluents by paramorphogenic form of *Aspergillus oryzae*, *Water Sci. Technol.* 37 (2012) 49–54, doi:10.2166/wst.2012.037.
- [7] D.V. Sriharsha, R.L. Kumar, J. Savitha, Immobilized fungi on *Luffa cylindrica*: An effective biosorbent for the removal of lead, *J. Taiwan Inst. Chem. Eng.* 80 (2017) 589–595, doi:10.1016/j.jtice.2017.08.032.
- [8] B. Saba, A.D. Christy, M. Jabeen, Kinetic and enzymatic decolorization of industrial dyes utilizing plant-based biosorbents: A review, *Environ. Eng. Sci.* 33 (9) (2016) 601–614, doi:10.1089/ees.2016.0038.
- [9] F.H.M. Souza, V.F.C. Leme, G.O.B. Costa, K.C. Castro, T.R. Giraldo, G.S.S. Andrade, Biosorption of rhodamine B using a low-cost biosorbent prepared from inactivated *Aspergillus oryzae* cells: kinetic, equilibrium and thermodynamic studies, *Water Air Soil Pollut* 231 (5) (2020) 242, doi:10.1007/s11270-020-04633-8.
- [10] M.C. Ncibi, A.M. Hamissa, A. Fathallah, M.H. Kortas, T. Baklouti, B. Mahjoub, M. Seffen, Biosorptive uptake of methylene blue using Mediterranean green alga *Enteromorpha* spp., *J. Hazard. Mater.* 170 (2009) 1050–1055, doi:10.1016/j.jhazmat.2009.05.075.
- [11] M. Peydayesh, A. Rahbar-Kelishami, Adsorption of methylene blue onto *Plantus orientalis* leaf powder: kinetic, equilibrium and thermodynamic studies, *J. Ind. Eng. Chem.* 202 (2014) 1493–1501, doi:10.1016/j.jiec.2014.05.010.
- [12] R. Han, Y. Wang, W. Yu, W. Zou, J. Shi, H. Liu, Biosorption of methylene blue from aqueous solution by rice husk in a fixed-bed column, *J. Hazard. Mater.* 141 (2007) 713–718, doi:10.1016/j.jhazmat.2006.07.031.
- [13] K.V. Kumar, K. Porkodi, Mass transfer, kinetics and equilibrium studies for the biosorption of methylene blue using *Paspalum notatum*, *J. Hazard. Mater.* 141 (2007) 214–226, doi:10.1016/j.jhazmat.2006.12.010.
- [14] N.B. Douissa, L. Bergaoui, S. Mansouri, R. Khiari, M.F. Mhenni, Macroscopic and microscopic studies of methylene blue sorption onto extracted celluloses from *Posidonia oceanica*, *J. Ind. Crops Prod.* 45 (2013) 106–113, doi:10.1016/j.indcrop.2012.12.007.
- [15] M.C. Ncibi, B. Mahjoub, M. Seffen, Kinetic and equilibrium studies of methylene blue biosorption by *Posidonia oceanica* (L.) fibers, *J. Hazard. Mater.* 139 (2007) 280–285, doi:10.1016/j.jhazmat.2006.06.029.
- [16] R. Dallel, A. Kesraoui, M. Seffeh, Biosorption of cationic dye onto “Phragmites australis” fibers: characterization and mechanism, *J. Environ. Chem. Eng.* 6 (2018) 7247–7256, doi:10.1016/j.jece.2018.10.024.
- [17] Y. Lakhri, M. Rbaa, B. Tuzun, A. Hichar, K. Ounine, F. Almalki, T.B. Hadda, A. Zarrouk, B. Lakhri, Synthesis, structural confirmation, antibacterial properties and bio-informatics computational analyses of new pyrrole based on 8-hydroxyquinoline, *J. Mol. Struct.* 1259 (2022) 132683, doi:10.1016/j.molstruc.2022.132683.
- [18] I.A.S. Al-Janabi, S.Ç. Yavuz, S. Köprü, M. Tapera, H. Kekeçmuhammed, S. Akkoç, B. Tüzün, Ş. Patat, E. Sarıpinar, Antiproliferative activity and molecular docking studies of new 4-oxothiazolidin-5-ylidene acetate derivatives containing guanyldiazone moiety, *J. Mol. Struct.* 1258 (2022) 132627, doi:10.1016/j.molstruc.2022.132627.
- [19] M. Rbaa, S. Haida, B. Tuzun, A. El Hassane, A. Kribii, Y. Lakhri, T.B. Hadda, A. Zarrouk, B. Lakhri, E. Berdimurodov (2022) Synthesis, characterization and bioactivity of novel 8-hydroxyquinoline derivatives: Experimental, molecular docking, DFT and POM analyses, *J. Mol. Struct.* 1258, 132688. <https://doi.org/10.1016/j.molstruc.2022.132688>
- [20] Ö. Dülger, F. Turak, K. Turhan, Sumac leaves as a novel low-cost adsorbent for removal of basic dye from aqueous solution, *ISRN Anal. Chem.* (2013), doi:10.1155/2013/210470.
- [21] J. Gülen, B. Akın, M. Özgür, Ultrasonic-assisted adsorption of methylene blue on sumac leaves, *Desal. Water Treat* 57 (20) (2015) 9286–9295, doi:10.1080/19443994.2015.1029002.
- [22] J. Sarma, A. Sarma, K.G. Bhattacharyya, Biosorption of commercial dyes on *Azadiracta indica* leaf powder: A case study with a basic dye Rhodamine B, *Ind. Eng. Chem. Res.* 47 (2008) 5433–5440, doi:10.1021/ie071266i.
- [23] M. Tüzen, A. Sarı, T.A. Saleh, Response surface optimization, kinetic and thermodynamic studies for effective removal of rhodamine B by magnetic AC/CeO<sub>2</sub> nanocomposite, *J. Environ. Manage.* 206 (2018) 170–177, doi:10.1016/j.jenvman.2017.10.016.
- [24] M.J. Frisch, G.W. Trucks, H.B. Schlegel, G.R. Scuseria, M.A. Robb, J.R. Cheeseman, G. Scalmani, V. Barone, B. Mennucci, G.A. Petersson, H. Nakatsuji, M. Caricato, X. Li, H.P. Hratchian, A.F. Izmaylov, J. Bloino, G. Zheng, J.L. Sonnenberg, M. Hada, M. Ehara, K. Toyota, R. Fukuda, J. Hasegawa, M. Ishida, T. Nakajima, Y. Honda, O. Kitao, H. Nakai, T. Vreven, J.A. Montgomery, J.E. Peralta, F. Ogliaro, M. Bearpark, J.J. Heyd, E. Brothers, K.N. Kudin, V.N. Staroverov, R. Kobayashi, J. Normand, K. Raghavachari, A. Rendell, J.C. Burant, S.S. Iyengar, J. Tomasi, M. Cossi, N. Rega, J.M. Millam, M. Klene, J.E. Knox, J.B. Cross, V. Bakken, C. Adamo, J. Jaramillo, R. Gomperts, R.E. Stratmann, O. Yazyev, A.J. Austin, R. Cammi, C. Pomelli, J.W. Ochterski, R.L. Martin, K. Morokuma, V.G. Zakrzewski, G.A. Voth, P. Salvador, J.J. Dannenberg, S. Dapprich, A.D. Daniels, O. Farkas, J.B. Foresman, J.V. Ortiz, J. Cioslowski, D.J. Fox, Gaussian 09, revision D.01, Gaussian Inc, Wallingford, 2009.
- [25] R. Dennington, T. Keith, J. Millam, GaussView, Semichem Inc., 2016 Version 6.
- [26] A.D. Becke, Density-functional thermochemistry. I. The effect of the exchange-only gradient correction, *J. Chem. Phys.* 96 (3) (1992) 2155–2160, doi:10.1063/1.462066.
- [27] D. Vautherin, D.T. Brink, Hartree-Fock calculations with Skyrme’s interaction. I. Spherical nuclei, *Physical Review C* 5 (3) (1972) 626, doi:10.1103/PhysRevC.5.626.
- [28] E.G. Hohenstein, S.T. Chill, C.D. Sherrill, Assessment of the performance of the M05–2X and M06–2X exchange-correlation functionals for noncovalent interactions in biomolecules, *J. Chem. Theory Comput.* 4 (12) (2008) 1996–2000, doi:10.1021/ct800308k.
- [29] Z. Kökbudak, S. Akkoç, H. Karataş, B. Tüzün, G. Aslan, Silico and In Vitro Antiproliferative Activity Assessment of New Schiff Bases, *ChemistrySelect* 7 (3) (2022) e202103679, doi:10.1002/slct.202103679.
- [30] M.A. Bhat, B. Tüzün, N.A. Alsaif, A.A. Khan, A.M. Naglah, Synthesis, characterization, molecular modeling against EGFR target and ADME/T analysis of novel purine derivatives of sulfonamides, *J. Mol. Struct.* 1257 (2022) 132600, doi:10.1016/j.molstruc.2022.132600.
- [31] M.S. Priya, P. Divya, R. Rajalakshmi, A review status on characterization and electrochemical behaviour of biomass derived carbon materials for energy storage supercapacitors, *Sustain. Chem. Pharm.* 16 (2020) 100243, doi:10.1016/j.scp.2020.100243.
- [32] F. Gündüz, B. Bayrak, Biosorption of malachite green from an aqueous solution using pomegranate peel: Equilibrium modelling, kinetic and thermodynamic studies, *J. Mol. Liq.* 243 (2017) 790–798, doi:10.1016/j.molliq.2017.08.095.
- [33] D. Saraydın, Y. Isikver, E. Karadag, Adsorption of Phenazine Dyes Using Poly(hydroxamic acid) Hydrogels from Aqueous Solutions, *Polym. Eng. Sci.* 58 (3) (2018) 310–318, doi:10.1002/pen.24574.
- [34] B. Acemioğlu, Removal of Fe (II) ions from aqueous solution by calabrian pinebark wastes, *Bioresour. Technol.* 93 (2004) 99–102, doi:10.1016/j.biortech.2003.10.010.
- [35] R. Li, N. Liang, X. Ma, B. Chen, F. Huang, Study on the adsorption behavior of glycerin from fatty acid methyl esters by a tertiary amine-type anion exchange resin, *J. Chromatogr. A* 1586 (2019) 62–71, doi:10.1016/j.chroma.2018.11.079.
- [36] Z.Ç. Okumuş, T.H. Doğan, Removal of Water from Biodiesel with Resin: Isothermal, Kinetic and Thermodynamic Investigation of Adsorption, *European Journal of Science and Technology* 15 (2019) 561–570, doi:10.31590/ejosat.535977.
- [37] F. Deniz, Bioremoval of a Model Synthetic Azo Dye from Aquatic Medium by *Zostera marina* L.: Biosorption System Modeling Studies, *Eskişehir Technical University Journal of Science and Technology C- Life Sciences and Biotechnology* 9 (1) (2020) 1–12.
- [38] T.M. Elmorsi, Z.H. Mohamed, W. Shopak, A.M. Ismaiel, Kinetic and Equilibrium Isotherms Studies of Adsorption of Pb(II) from Water onto Natural Adsorbent, *Journal of Environmental Protection* 5 (2014) 1667–1681, doi:10.4236/jep.2014.517157.
- [39] W. Rudzinski, W. Plazinski, Kinetics of Solute Adsorption at Solid/Solution Interfaces: A Theoretical Development of the Empirical Pseudo-First and Pseudo-Second Order Kinetic Rate Equations, Based on Applying the Statistical Rate Theory of Interfacial Transport, *The Journal of Physical Chemistry B* 110 (2006) 16514–16525, doi:10.1021/jp061779n.
- [40] S. Akkoç, B. Tüzün, A. Özalp, Z. Kökbudak, Investigation of structural, electronic and in vitro cytotoxic activity properties of some heterocyclic compounds, *Journal of Molecular Structure* 1246 (2021) 131127, doi:10.1016/j.molstruc.2021.131127.
- [41] K. Karrouchi, S. Fattach, B. Tüzün, S. Radi, A.I. Alharthi, H.A. Ghabbour, Y.N. Mabkhot, M.E.A. Faouzi, M. Ansar, Y. Garcia, Synthesis, crystal structure, DFT,  $\alpha$ -glucosidase and  $\alpha$ -amylase inhibition and molecular docking studies of (E)-N’-(4-chlorobenzylidene)-5-phenyl-1H-pyrazole-3-carbohydrazide, *Journal of Molecular Structure* 1245 (2021) 131067, doi:10.1016/j.molstruc.2021.131067.
- [42] S. Sagdinc, H. Pir, Spectroscopic and DFT studies of flurbiprofen as dimer and its Cu (II) and Hg (II) complexes, *Spectrochimica Acta Part A: Molecular and Biomolecular Spectroscopy* 73 (1) (2009) 181–194, doi:10.1016/j.saa.2009.02.022.
- [43] L. Padmaja, C. Ravikumar, D. Sajan, I. Hubert Joe, V.S. Jayakumar, G.R. Pettit, O. Faurkov Nielsen, Density functional study on the structural conformations and intramolecular charge transfer from the vibrational spectra of the anti-cancer drug combretastatin-A2, *Journal of Raman Spectroscopy: An International Journal for Original Work in all Aspects of Raman Spectroscopy, Including Higher Order Processes, and also Brillouin and Rayleigh Scattering* 40 (4) (2009) 419–428, doi:10.1002/jrs.2145.
- [44] D. Majumdar, B. Tüzün, T.K. Pal, R.V. Saini, K. Bankura, D. Mishra, Structurally diverse heterobimetallic Pb (II)-Salen complexes mechanistic notion of cytotoxic activity against neuroblastoma cancer cell: Synthesis, characterization, protein-ligand interaction profiler, and intuitions from DFT, *Polyhedron* 210 (2021) 115504, doi:10.1016/j.poly.2021.115504.
- [45] M. Rbaa, A. Oubih, H. Hajji, B. Tüzün, A. Hichar, E. Berdimurodov, M.A. Ajana, A. Zarrouk, B. Lakhri, (2021) Synthesis, bioinformatics and biological evalu-

- ation of novel pyridine based on 8-hydroxyquinoline derivatives as antibacterial agents: DFT, molecular docking and ADME/T studies. *Journal of Molecular Structure*, 1244, 130934. <https://doi.org/10.1016/j.molstruc.2021.130934>
- [46] A. Huseynzada, M. Mori, F. Meneghetti, A. Israyilova, G. Tuzun, K. Sayin, ... V. Abbasov, Synthesis, crystal structure, Hirshfeld surface, computational and antibacterial studies of a 9-phenanthrenecarboxaldehyde-based thiodihydropyrimidine derivative, *Journal of Molecular Structure* 1267 (2022) 133571, doi:[10.1016/j.molstruc.2022.133571](https://doi.org/10.1016/j.molstruc.2022.133571).
- [47] A.T. Bilgiçli, T. Kandemir, B. Tüzün, R. Arıdurdu, A. Günsel, Ç. Abak, M.N. Yarasir, G. Arabaci, Octa-substituted Zinc (II), Cu (II), and Co (II) phthalocyanines with 1-(4-hydroxyphenyl) propane-1-one: Synthesis, sensitive protonation behaviors, Ag (I) induced H-type aggregation properties, antibacterial-antioxidant activity, and molecular docking studies, *Applied Organometallic Chemistry* 35 (10) (2021) e6353, doi:[10.1002/aoc.6353](https://doi.org/10.1002/aoc.6353).
- [48] S.Ç. Yavuz, S. Akkoç, B. Tüzün, O. Şahin, E. Saripinar, Efficient synthesis and molecular docking studies of new pyrimidine-chromeno hybrid derivatives as potential antiproliferative agents, *Synthetic Communications* 51 (14) (2021) 2135–2159, doi:[10.1080/00397911.2021.1922920](https://doi.org/10.1080/00397911.2021.1922920).
- [49] D. Glossman-Mitnik, Computational study of the chemical reactivity properties of the Rhodamine B molecule, *Procedia Computer Science* 18 (2013) 816–825, doi:[10.1016/j.procs.2013.05.246](https://doi.org/10.1016/j.procs.2013.05.246).
- [50] A. Kausar, R. Shahzad, S. Asim, S. BiBi, J. Iqbal, N. Muhammad, M. Sillanpaa, I.U. Din, Experimental and theoretical studies of Rhodamine B direct dye sorption onto clay-cellulose composite, *Journal of Molecular Liquids* 328 (2021) 115165, doi:[10.1016/j.molliq.2020.115165](https://doi.org/10.1016/j.molliq.2020.115165).
- [51] B. Tüzün, J. Bhawsar, Quantum chemical study of thiazole derivatives as corrosion inhibitors based on density functional theory, *Arabian Journal of Chemistry* 14 (2) (2021) 102927, doi:[10.1016/j.arabjc.2020.102927](https://doi.org/10.1016/j.arabjc.2020.102927).
- [52] A. Mermer, M.V. Bulbul, S.M. Kalender, I. Keskin, B. Tuzun, O.E. Eyupoglu, Benzotriazole-oxadiazole hybrid Compounds: Synthesis, anticancer Activity, molecular docking and ADME profiling studies, *Journal of Molecular Liquids* 359 (2022) 119264, doi:[10.1016/j.molliq.2022.119264](https://doi.org/10.1016/j.molliq.2022.119264).